A Novel Nonlinear Piezoelectric Energy Harvesting System Based on Linear-Element Coupling: Design, Modeling and Dynamic Analysis

Shengxi Zhou [1,3,*], **Bo Yan** [2,*] **and Daniel J. Inman** [3]

[1]   School of Aeronautics, Northwestern Polytechnical University, Xi'an 710072, China
[2]   Faculty of Mechanical Engineering & Automation, Zhejiang Sci-Tech University, Hangzhou 310018, China
[3]   Department of Aerospace Engineering, University of Michigan, Ann Arbor, MI 48109-2140, USA;
      daninman@umich.edu
[*]   Correspondence: zhoushengxi@nwpu.edu.cn (S.Z.); yanbo@zstu.edu.cn (B.Y.);
      Tel.: +86-131-5217-5925 (S.Z.); +86-0571-8684-3347 (B.Y.)

check for updates

Abstract: This paper presents a novel nonlinear piezoelectric energy harvesting system which consists of linear piezoelectric energy harvesters connected by linear springs. In principle, the presented nonlinear system can improve broadband energy harvesting efficiency where magnets are forbidden. The linear spring inevitably produces the nonlinear spring force on the connected harvesters, because of the geometrical relationship and the time-varying relative displacement between two adjacent harvesters. Therefore, the presented nonlinear system has strong nonlinear characteristics. A theoretical model of the presented nonlinear system is deduced, based on Euler-Bernoulli beam theory, Kirchhoff's law, piezoelectric theory and the relevant geometrical relationship. The energy harvesting enhancement of the presented nonlinear system (when n = 2, 3) is numerically verified by comparing with its linear counterparts. In the case study, the output power area of the presented nonlinear system with two and three energy harvesters is 268.8% and 339.8% of their linear counterparts, respectively. In addition, the nonlinear dynamic response characteristics are analyzed via bifurcation diagrams, Poincare maps of the phase trajectory, and the spectrum of the output voltage.

Keywords: linear elements; coupled system; modeling; energy harvesting; nonlinear dynamics

1. Introduction

In order to solve the challenging issue of the energy supply for wireless sensors, small portable devices and MEMS, piezoelectric vibration energy harvesting based on the piezoelectric effect has been receiving more and more attention over the past two decades [1–10]. Meanwhile, piezoelectric vibration energy harvesting will positively promote the development of the structural health monitoring and the precision actuation [11–18]. Up to now, many different kinds of linear resonance based piezoelectric vibration energy harvesters have been designed, modeled, simulated and experimentally tested to investigate their energy harvesting performance [19–24]. However, these resonance based linear piezoelectric vibration energy harvesters are very sensitive to the external excitation frequency, which leads to the reduced capacity of vibration energy harvesting when they are subjected to a wide range of excitation frequencies. This issue has been inspiring many researchers to focus on widening the operating bandwidth of the vibration energy harvesters and enhancing their energy harvesting performance based on the active and adaptive frequency-tuning schemes [25–34].

Currently, intensive investigation is focusing on magnet-based nonlinear energy harvesting in the purpose of widening the operating frequency range and enhancing the energy harvesting performance.

It was demonstrated that magnet-based nonlinear monostable energy harvesters have a wider effective bandwidth and a higher energy harvesting efficiency than their linear counterparts [35–39]. What's more, the advantages of high-energy interwell oscillations and the broadband operating frequency range of the bistable configurations have been employed to harvest energy from broadband base excitations [40–46]. Recently, tristable energy harvesters with suitable design parameters were introduced and they experimentally exhibited a better energy harvesting performance compared to bistable energy harvesters under a very low level excitation [47–53]. These magnet-based nonlinear energy harvesters have been verified that they have an excellent energy harvesting performance and the broadband characteristics. However, in some special application areas (where magnets have the undesirable influence to the host objects or ambient environment), magnets are forbidden. Therefore, investigation of the non-magnet based vibration energy harvesting enhancement technique is necessary and meaningful.

For the non-magnet based vibration energy harvesting enhancement technique, Leland and Wright [54] presented a resonance-changeable piezoelectric vibration energy harvester with an adjustable axial preload. This harvester provides a wider operating frequency range than that of traditional linear energy harvesters. Shahruz et al. [55] presented a broadband piezoelectric vibration energy harvesting system by gathering several linear energy harvesters with different resonant frequencies together. Kim et al. [56] and Wu et al. [57] separately proposed a two degree of freedom (2-DOF) energy harvesting system, and their results showed that such systems have two peak displacement amplitudes at two different resonant frequencies causing a wider operating frequency range than that of the linear 1-DOF energy harvester. Kuch and Karami [58] provided a theoretical model of a nonlinear hybrid rotary-translational energy harvester and explored the application for powering heart pacemakers. Liu et al. [59] designed a bistable piezoelectric energy harvester based on a buckled spring-mass system, and their results show that a maximum power of 16 mW could be obtained for a 0.3 g chirp excitation. Chen et al. [60,61] utilized the internal resonance mechanism to enhance vibration-based energy harvesting, and they made a theoretical analysis via nonlinear methods. Xu and Tang [62] developed a cantilever-pendulum energy harvesting system, which could harvest vibration energy of excitations from three directions in simulation. Li et al. [63] numerically and experimentally verified the broadband characteristics of a compressive-mode energy harvester. Wei and Jing [64] proposed a nonlinear energy harvesting system via a lever system combined with an X-shape supporting structure, and the numerical results show that this system provides a great flexibility and/or a unique tool for tuning and improving energy harvesting efficiency via matching excitation frequencies and covering a wider frequency range.

Previous research theoretically and experimentally verified on the enhanced performance of the non-magnet based vibration energy harvesting technique [54–64]. More importantly, non-magnet based vibration energy harvesting has an irreplaceable application potential in some special fields where magnets are forbidden. Meanwhile, more research and investigations about the non-magnet based vibration energy harvesting technique are need to promote the development and application of vibration energy harvesting. Therefore, it is meaningful to present new concepts or structures based non-magnet based nonlinear energy harvesting technique to enhance vibration energy harvesting performance.

This paper presented a novel nonlinear piezoelectric energy harvesting system (NPEHS) based on linear-element coupling, and it contains linear piezoelectric energy harvesters connected by linear springs. In Section 2, a theoretical model of the presented NPEHS is derived based on Euler-Bernoulli beam theory, Kirchhoff's law, piezoelectric theory, and the assumed geometrical relationship. In Section 3, case study is provided. In Section 4, the nonlinear dynamic response characteristics of the presented NPEHS are analyzed via bifurcation diagrams, Poincare maps of the phase trajectory, and the spectrum of the output voltage. Finally, key conclusions are presented.

2. Concept and Modeling

The idea of the presented NPEHS is based on the linear element coupled system, as its schematic diagram shown in Figure 1. The equivalent model of each linear energy harvester is surrounded by the closed blue dotted line, which was explored in Ref. [3]. Although each independent energy harvester has linear characteristics, based on coupled dynamic behaviors [65–67], the whole system will exhibit nonlinear characteristics when two adjacent linear energy harvesters are connected by linear springs ($K_1, \ldots K_{n-1}$ stand for their stiffness). Figure 2 shows the structure diagram of the presented NPEHS. In principle, the NPEHS contains n linear piezoelectric energy harvesters with different resonant frequencies, and they are connected by $n-1$ linear springs. The base excitation is imposed in the z direction, which is the same direction of the bending vibration of each energy harvester of the NPEHS. All the linear springs are connected in the y direction (width direction of each energy harvester). The NPEHS will exhibit nonlinear dynamic response characteristics when it is subjected to an excitation, because the nonlinear spring force is inevitably produced by the linear springs (which are disproportionately extended by the different vibration displacements from two connected adjacent energy harvesters in the system). The bending stiffness for a cantilever beam with rectangular cross section is $EI = \frac{bEh^3}{12}$. Therefore, the ratio of the bending stiffness for the lateral motion (y direction) EI_y and the bending stiffness for the transverse motion (z direction) EI_z is $\frac{EI_y}{EI_z} = \left(\frac{b}{h}\right)^2$. In this paper, the width b of the substrate is 65 times more than of the thickness h, which will be given in Table 1 in Section 3. Therefore, EI_y is more than 4000 times of EI_z. In this case, the lateral motion is negligible. It is truly that the harvester will become softer in the y direction as the stiffness of the connected spring increases. However, the stiffness of the connected spring is much smaller than the lateral equivalent stiffness in this study.
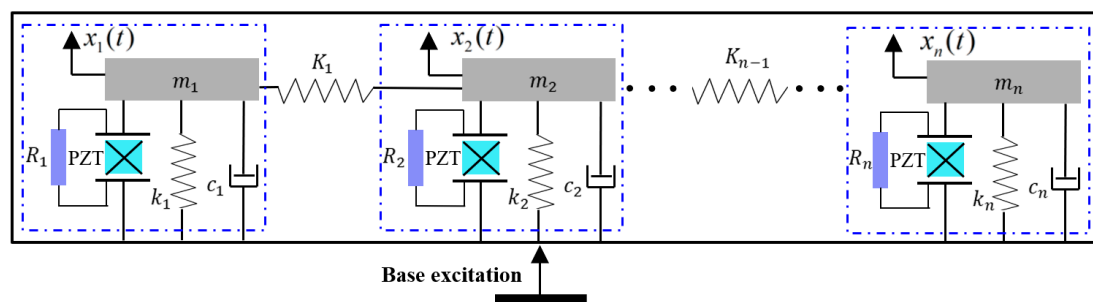

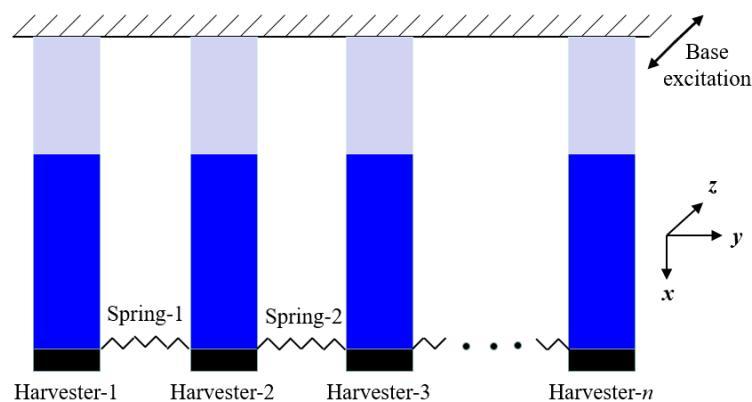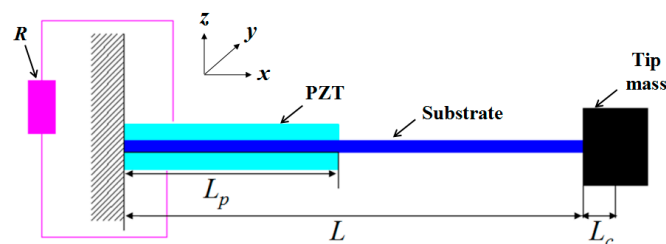**Figure 1.** Schematic diagram of the NPEHS.

Figure 2. Structural diagram of the NPEHS.

	L	L_p	L_c	b	h_s	h_p
Harvester-1	80	20	5	15	0.10	0.5
Harvester-2	80	20	5	15	0.18	0.5
Harvester-3	80	20	5	15	0.23	0.5

In this paper, a theoretical model of the NPEHS is deduced based on Euler-Bernoulli beam theory, piezoelectric theory, Kirchhoff's law, and the relevant geometric relationship. In the theoretical model, we assume that all the linear springs are elastic and own the constant stiffness.

In order to obtain the theoretical model of the presented NPEHS under a base excitation, the electromechanical governing equations of each linear energy harvester should be firstly built based on Euler-Bernoulli beam theory, proportional damping, piezoelectric theory, and Kirchhoff's law. In this study, each linear piezoelectric energy harvester in the proposed system has the non-uniform cross-section as its schematic shown in Figure 3. The length of the substrate and the piezoelectric layers of the drawn harvester is L and L_p (in the x direction), respectively. The thickness of the former and the latter is h_s and h_p (in the z direction), respectively. L_c is the half length of the cuboid tip mass block. R is the external resistance load. b is the width (in the y direction) of both the substrate and the piezoelectric layers.

Figure 3. Linear piezoelectric energy harvester with the non-uniform cross-section in the NPEHS.

As one of the mechanisms for energy conversion, piezoelectric laminates bonded to cantilever beams have been widely studied. The piezoelectric constitutive equations are used to describe their electromechanical behavior, as shown in Appendix A. For a thin cantilever beam with the uniform cross-section, these parameters are given by Erturk and Inman [3]. Based on Euler-Bernoulli beam theory, piezoelectric effect, and Kirchhoff's law, the electromechanical governing equations of a linear piezoelectric energy harvester with non-uniform cross-section can be written as:

$$EI\frac{\partial^4 v(x,t)}{\partial x^4} + c_s\frac{\partial^5 v(x,t)}{\partial x^4 \partial t} + c_m\frac{\partial v(x,t)}{\partial t} + m\frac{\partial^2 v(x,t)}{\partial t^2} - \vartheta V(t)\left[\frac{d\delta(x)}{dx} - \frac{d\delta(x-L_p)}{dx}\right] = \ldots$$
$$-\left[m + M_{tip}\delta(x-L) + M_{tip}L_c\frac{d\delta(x-L)}{dx}\right]\frac{\partial^2 v_b(t)}{\partial t^2}$$

(1)

$$C_p\frac{dV(t)}{dt} + \frac{V(t)}{R} + \vartheta\int_0^{L_p}\frac{\partial^3 v(x,t)}{\partial x^2 \partial t}dx = 0$$

(2)

where $v_b(t)$ is the base displacement used as the excitation; $v(x,t)$ is the displacement of the energy harvester relative to the base; $V(t)$ is the output voltage across R; c_m and c_s are the external damping coefficient (mass-proportional damping) and the internal damping coefficient of the composite structure (stiffness-proportional damping), respectively. M_{tip} is the tip mass; the equivalent capacitance of the piezoelectric layers for parallel connection in this paper is $C_p = 2\varepsilon_{33}^S bL_p/h_p$; the electromechanical coupling term is $\vartheta = e_{31}b(h_s + h_p)$ for parallel connection of the piezoelectric layers; m and EI are the mass per unit length of and the bending stiffness of the energy harvester, respectively. They depend on the location of the piezoelectric layers, as follows: $m_1 = b\rho_s h_s + 2b\rho_p h_p$,

for $0 \le x \le L_p$; $m_2 = b\rho_s h_s$, for $L_p < x \le L$; $EI_1 = \frac{2}{3}b\left(\frac{E_s h_s^3}{8} + E_p\left(\left(h_p + \frac{h_s}{2}\right)^3 - \frac{h_s^3}{8}\right)\right)$, for $0 \le x \le L_p$;

$EI_2 = \frac{bE_s h_s^3}{12}$, for $L_p < x \le L$. ρ_p and ρ_s are the density of the piezoelectric layers and the substrate, respectively; h_p and h_s are the thickness of the piezoelectric layers and the substrate, respectively; E_p and E_s are the Young's modulus of the piezoelectric layers and the substrate, respectively.

The relative displacement $v(x, t)$ in the physical coordinates can be written as the combination of the mode shape $\phi_i(x)$ and the modal coordinates $r_i(t)$, as follows:

$$v(x, t) = \sum_{i=1}^n \phi_i(x) r_i(t) \tag{3}$$

Since the piezoelectric layers are not covering the whole beam, the mode shape of the energy harvester is comprised of two different parts:

$$(\phi(x))_1 = A_1 \sin(\beta_1 x) + B_1 \cos(\beta_1 x) + C_1 \sinh(\beta_1 x) + D_1 \cosh(\beta_1 x), \text{ for } 0 \le x \le L_p \tag{4}$$

$$(\phi(x))_2 = A_2 \sin(\beta_2 x) + B_2 \cos(\beta_2 x) + C_2 \sinh(\beta_2 x) + D_2 \cosh(\beta_2 x), \text{ for } L_p < x \le L \tag{5}$$

The eigenvalue equations are given by:

$$EI_1(\phi)_1^{iv} - m_1\omega^2(\phi)_1 = 0 \tag{6}$$

$$EI_2(\phi)_2^{iv} - m_2\omega^2(\phi)_2 = 0 \tag{7}$$

where $\omega = \beta_1^2\sqrt{\frac{EI_1}{m_1}} = \beta_2^2\sqrt{\frac{EI_2}{m_2}}$.

At the clamped end, the displacement and the angle of rotation should be zero. Since the linear piezoelectric energy harvester is considered to meet Euler-Bernoulli beam theory, the condition of the displacement, the angle of rotation, the bending moment and the shear force are continuous at the joint position of two different parts.

Based on boundary conditions shown in Appendix A, orthogonality conditions of the normalized mode shapes can be used to get the final dynamic model:

$$\begin{aligned}
&\int_0^{L_p} (\phi_i(x))_1 m_1 (\phi_j(x))_1 dx + \int_{L_p}^L (\phi_i(x))_2 m_2 (\phi_j(x))_2 dx + (\phi_i(L))_2 M_{tip}(\phi_j(L))_2 + \dots \\
&(\phi_i(L))_2'(I_t + M_{tip}L_c^2)(\phi_j(L))_2' + (\phi_i(L))_2 M_{tip}L_c(\phi_j(L))_2' + \dots \\
&(\phi_i(L))_2' M_{tip}L_c(\phi_j(L))_2 = \delta_{ij}
\end{aligned} \tag{8}$$

$$\int_0^{L_p} (\phi_i(x))_1'' EI_1 (\phi_j(x))_1'' dx + \int_{L_p}^L (\phi_i(x))_2'' EI_2 (\phi_j(x))_2'' dx = \delta_{ij}\omega^2 \tag{9}$$

where i and j present the vibration modes. δ_{ij} is the Kronecker delta, which is defined as unity when i is equal to j and zero otherwise.

In principle, the relative displacement $v(x, t)$ in the physical coordinates consists of an unlimited number of the mode shape $\phi_i(x)$ and the modal coordinates $r_i(t)$ ($i = 1, 2, 3, \dots, n$), as shown in Equation (3). Meanwhile, the first vibration mode of piezoelectric energy harvesters was theoretically and experimentally verified to play an overwhelming role in vibration energy harvesting [1,3,8,68,69]. Therefore, this study only considers the first vibration mode. The electromechanical governing equations is reduced to only include the first vibration mode of the energy harvester. Based on above derivation, the electromechanical governing equations in the first-order modal coordinates are obtained, as follows:

$$\ddot{r}(t) + 2\zeta\omega\dot{r}(t) + \omega^2 r(t) - \theta V(t) = f(t) \tag{10}$$

$$C_p\dot{V}(t) + \frac{V(t)}{R} + \theta\dot{r}(t) = 0 \tag{11}$$

where the modal electromechanical coupling coefficient $\theta = \vartheta((\phi(L_p))'_1 - (\phi(0))'_1)$. ζ is the equivalent modal damping ratio, which is based on empirical values in experiments and models [3,70,71].

The modal force $f(t)$ is defined as the following equation:

$$f(t) = -\left[\int_0^{L_p} m_1(\phi(x))_1 dx + \int_{L_p}^L m_2(\phi(x))_2 dx + M_{tip}(\phi(L))_2 + M_{tip}L_c(\phi(L))'_2\right]\frac{\partial^2 v_b(t)}{\partial t^2} \tag{12}$$

By far, the modeling process of the linear piezoelectric energy harvester is completed. In order to get the complete theoretical model of the proposed system, the connected springs should be considered. The detailed geometrical relationship of two adjacent energy harvesters is assumed as the schematic diagram depicted in Figure 4. Since the vibration direction is in the z direction, D_i is the original length of spring-i. $v_i(L,t)$ and $v_{i+1}(L,t)$ are the tip displacement of harvester-i and harvester-$(i+1)$ relative to the base, respectively.
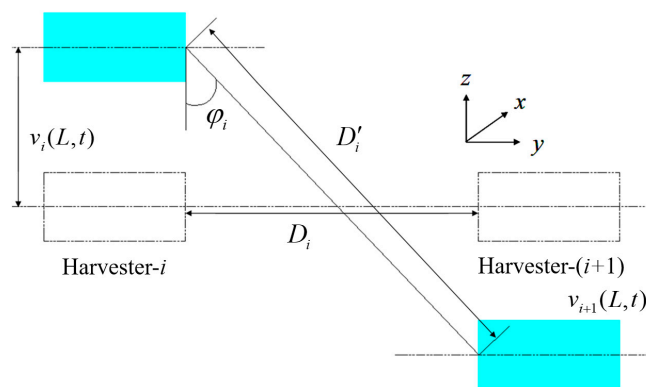

Figure 4. Relative geometrical position of two adjacent harvesters.

As shown in Figure 4, the transient length of spring-i is D'_i, as follows:

$$D'_i = \sqrt{D_i^2 + (v_i(L,t) - v_{i+1}(L,t))^2} \tag{13}$$

The transient included angle φ_i between spring-i and the z axis can be written as:

$$\cos(\varphi_i) = \frac{v_i(L,t) - v_{i+1}(L,t)}{D'_i} \tag{14}$$

Assuming all the springs being elastic and owning constant stiffness, based on Hooke's law, the effective force generated by spring-i upon harvester-i is its component force in the z direction, as follows:

$$F_{(i+1)i} = K_i(D'_1 - D_i)\cos(\varphi_i) \tag{15}$$

where K_i is the linear stiffness of spring-i.

Similarly, the effective spring force between any two adjacent energy harvesters can be calculated. In this study, each energy harvester separately connects with an external load resistance. Therefore, there are n mutually independent electrical equations based on Kirchhoff's law. Finally, the theoretical

model of the NPEHS with n linear energy harvesters in the first-order modal coordinate system are obtained and described by the following equations:

$$\begin{cases} \begin{cases} \ddot{r}_1(t) + 2\zeta_1\omega_1\dot{r}_1(t) + \omega_1^2 r_1(t) - \theta_1 V_1(t) + (\phi(L))_{1(2)} F_{21} = f_1(t) \\ (C_p)_1 \dot{V}_1(t) + \frac{V_1(t)}{R_1} + \theta_1 \dot{r}_1(t) = 0 \end{cases} \\ \begin{cases} \ddot{r}_2(t) + 2\zeta_2\omega_2\dot{r}_2(t) + \omega_2^2 r_2(t) - \theta_2 V_2(t) - (\phi(L))_{2(2)} F_{21} + (\phi(L))_{2(2)} F_{32} = f_2(t) \\ (C_p)_2 \dot{V}_2(t) + \frac{V_2(t)}{R_2} + \theta_2 \dot{r}_2(t) = 0 \end{cases} \\ \begin{cases} \cdots \end{cases} \\ \begin{cases} \cdots \end{cases} \\ \begin{cases} \ddot{r}_n(t) + 2\zeta_n\omega_n\dot{r}_n(t) + \omega_n^2 r_n(t) - \theta_n V_n(t) - (\phi(L))_{n(2)} F_{n(n-1)} = f_n(t) \\ (C_p)_n \dot{V}_n(t) + \frac{V_n(t)}{R_n} + \theta_n \dot{r}_n(t) = 0 \end{cases} \end{cases} \tag{16}$$

where the subscripts 1, 2, ..., n stand for the number of energy harvesters in the NPEHS. For example, $F_{i(i-1)}$ is the effective force generated by spring-$(i-1)$ upon harvester-$(i-1)$. Meanwhile, $(\phi(L))_{i(2)}$ stands for the mode shape of the second part (at the location of L) of the i-th energy harvester.

3. Case Study for Verifying Energy Harvesting Improvement

In the last section, the theoretical model of the NPEHS is derived. In order to verify its energy harvesting enhancement, the NPEHS-1 ($n = 2$) and the NPEHS-2 ($n = 3$) are investigated below, and their diagrams are shown in Figure 5a,b, respectively. The geometrical parameters of each harvester are shown in Table 1. The material property parameters are depicted in Table 2. In detail, beryllium bronze (UNS C1720) is selected as the substrate, whose density and Young's modulus are 8250 kg/m^3 and 125 GPa, respectively. Piezoelectric laminate properties are referred to [45]. The tip mass of each harvester is made of the same material with the substrate, and its size is $15 \times 10 \times 5$ mm^3. The natural frequency of harvester-1, harvester-2 and harvester-3 is calculated to be 2.59 Hz, 6.18 Hz and 8.86 Hz, respectively. In this section, 0.2 g is selected as the harmonic base excitation level. In addition, linearly increasing frequency excitation simulations with a low rate of frequency change (0.03 Hz/s) are performed.
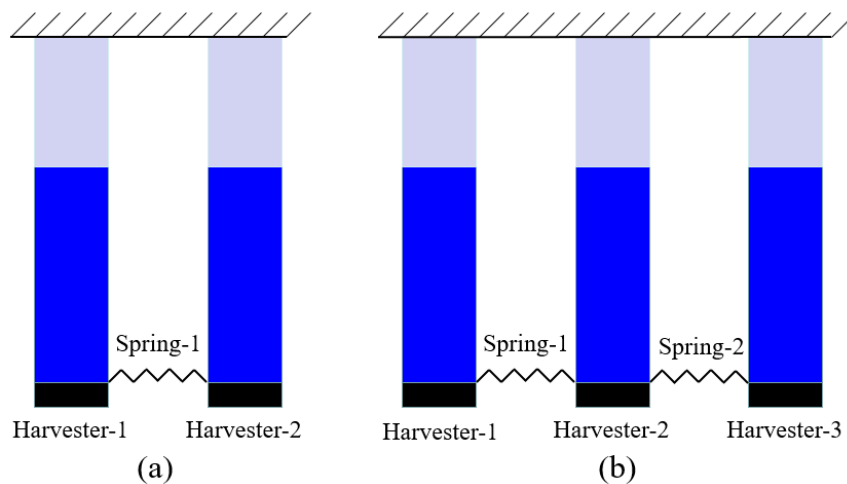

Figure 5. Diagrams of (**a**) the NPEHS-1; (**b**) the NPEHS-2.

Table 2. Material property parameters.

Substrate		
Parameter	**Symbol**	**Value**
Young's modulus	E_s	125 GPa
Density	ρ_s	8250 kg/m^3
Piezoelectric layers		
Young's modulus	E_p	63 GPa
Density	ρ_p	7700 kg/m^3
Coupling coefficient	d_{31}	-285×10^{-12} C/N
Permittivity constant	ε_{33}^S	3200 ε_0
Permittivity of free space	ε_0	8.854×10^{-12} F/m

Under a harmonic base excitation, the output power of each energy harvester can be calculated by using the equation $P = \left(\frac{\sqrt{2}}{2} V_A \right)^2 / R$ (V_A is the output voltage amplitude). By far, there is no generally applicable criterion to determine the energy harvesting capacity. Over a wide range of excitation frequencies, the total area of the output power of an energy harvesting system may stand for its energy harvesting capacity [21]. In addition, the specific value of the energy harvesting improvement of the NPEHS over the linear energy harvesters is very important to estimate its contribution. Therefore, the output power area ratio γ can be used to evaluate the energy harvesting performance of the NPEHS relative to its linear counterparts, as follows:

$$\gamma = P/P_L \tag{17}$$

where P and P_L are the total output power area of the NPEHS and the corresponding linear counterparts, respectively.

3.1. The NPEHS-1 with Two Energy Harvesters

Compared with energy harvesters in the system, the connected linear springs are easier to optimize and select. If finding the maximum γ is the optimization objective, the connected linear springs can be optimized by using Genetic Algorithm, Particle Swarm Optimization or other optimization algorithms. A simplest way to optimize the connected linear springs is to calculate the energy harvesting performance over a wide range of parameter values of the springs, and then we can find the best parameters of the springs. In detail, γ of the NPEHS-1 with different springs (initial length and stiffness can be confined in a certain range) can be calculated. However, the other parameters of the NPEHS-1 should be set as constant, when we optimize the springs.

Figure 6 shows the output power area ratio γ of the NPEHS-1 along with different D_1 (ranging from 6 mm to 134 mm) and K_1 (ranging from 10 N/m to 650 N/m). In detail, Figure 6a,b are the top view and the oblique view of the output power area ratio γ along with different D_1 and K_1 of the NPEHS-1. The brighter the area stand for the higher γ. It is found that the optimal initial length D_1 and the optimal stiffness K_1 of the connected spring-1 in the NPEHS-1 are 128 mm and 370 N/m, respectively. In this case, γ is 2.688, which means that the output power area of the NPEHS-1 is 268.8% of that of its linear counterparts. The ratio of the physical stiffness of the harvester-i and the stiffness of connected spring can be approximate to $\frac{k_i}{K_i} = \frac{\omega_i^2}{(\phi(L))_{i(2)}K_i}$, and $\frac{\omega_1^2}{(\phi(L))_{1(2)}K_1}$ and $\frac{\omega_2^2}{(\phi(L))_{2(2)}K_1}$ are 0.086 and 0.70, respectively. As the output voltage shown in Figure 7, the NPEHS-1 with optimal spring-1 can efficiently harvest vibration energy over a wider range of excitation frequencies. In addition, the response voltage curve of coupled harvesters in the NPEHS-1 shows obvious nonlinear dynamic response characteristics, which can be identified by comparing with the response voltage curve of linear harvesters in the same plots. The energy harvesting enhancement of the NPEHS-1 can be found in the output power curves, as shown in Figure 8.
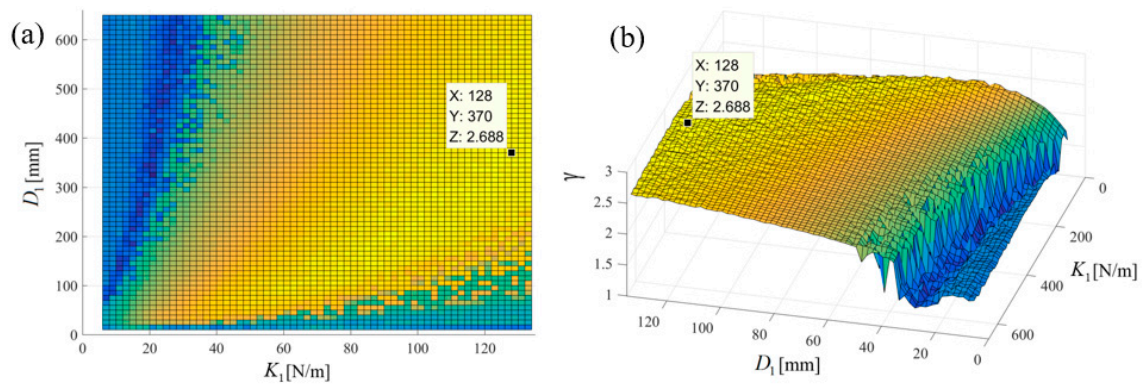
Figure 6. The output power area ratio γ along with different D_1 and K_1 of the NPEHS-1: (**a**) Top view; (**b**) oblique view.
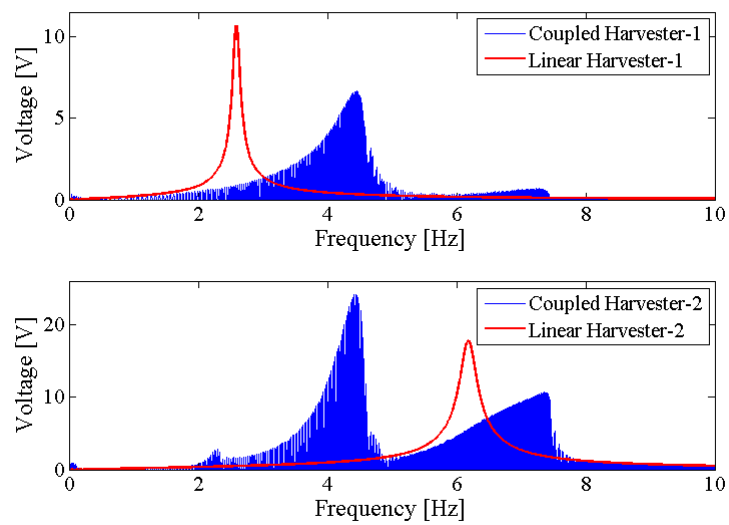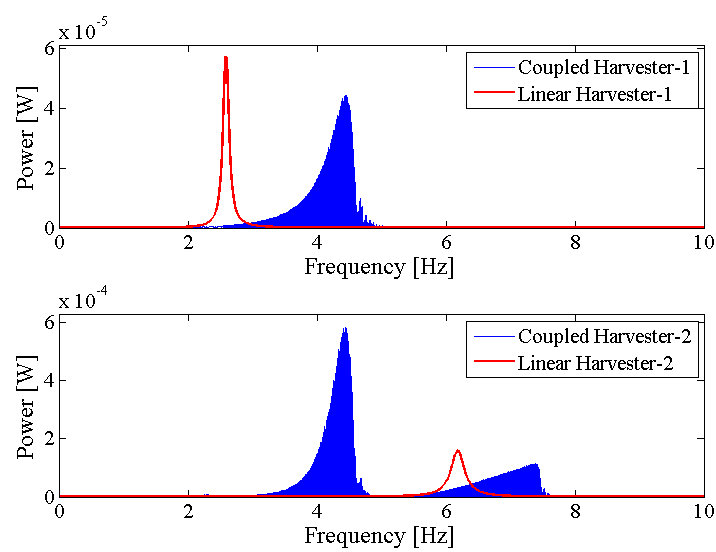

Figure 7. Output voltage of the NPEHS-1.

Figure 8. Output power of the NPEHS-1.

If the excitation frequency range where the output power is larger than 20 μW is considered to be effective, the effective bandwidth of the coupled harvester-1 is 0.45 Hz which is 321% of that (0.14 Hz) of the linear harvester-1, as shown in the first plot of Figure 8. Meanwhile, the bandwidth of the coupled harvester-2 is 4.86 Hz, while the bandwidth shrinks to be 0.86 Hz in its linear case, as shown in the second plot of Figure 8. This demonstrates that the bandwidth of the NPEHS-1 is wider than its linear counterparts. Figure 9 shows the different output power area ratio γ of the NPEHS-1 subject to different load resistance R (ranging from 100 Ω to 10^8 Ω), and each γ is larger than 1.9. These results further verify the improvement of the energy harvesting performance of the NPEHS-1.

Figure 9. Output power area ratio of the NPEHS-1 versus load resistance.

3.2. The NPEHS-2 with Three Energy Harvesters

In order to further examine the energy harvesting enhancement of the proposed system, the NPEHS-2 which consists of harvester-1, harvester-2, harvester-3, spring-1 and spring-2 is studied. Based on calculation, 320 N/m and 78 mm are the optimal stiffness and the optimal initial length of spring-1, respectively. 180 N/m and 8 mm are the optimal stiffness and the optimal initial length of spring-2, respectively. The ratio of the physical stiffness of the harvester-3 and the stiffness of spring-2 is about 3.371. The comparison of the NPEHS-2 and its linear counterparts is shown in Figures 10 and 11. The NPEHS-2 exhibits nonlinear dynamic response characteristics, since the voltage response curves in Figure 10 have obvious frequency-jump phenomena [35–39]. Such nonlinear characteristics can efficiently improve the vibration energy harvesting capacity. In this case, the output power area ratio γ is 3.398, which is larger than that of the NPEHS-1. If the excitation frequency range where the output power is larger than 20 μW is considered to be effective, the effective bandwidth of the coupled harvester-1, the coupled harvester-2, and the coupled harvester-3 of the NPEHS-1 is 0.52 Hz, 3.30 Hz and 3.51 Hz, respectively, as the output power shown in Figure 11. However, the effective bandwidth of the linear harvester-1, the linear harvester-2 and the linear harvester-3 is only 0.14 Hz, 0.86 Hz and 1.53 Hz, respectively. Figure 12 shows γ of the NPEHS-2 subject to different load resistance R (ranging from 100 Ω to 10^8 Ω), and each γ is larger than 2.6. These results demonstrate that the optimized NPEHS with three energy harvesters has a better energy harvesting performance than its linear counterparts.
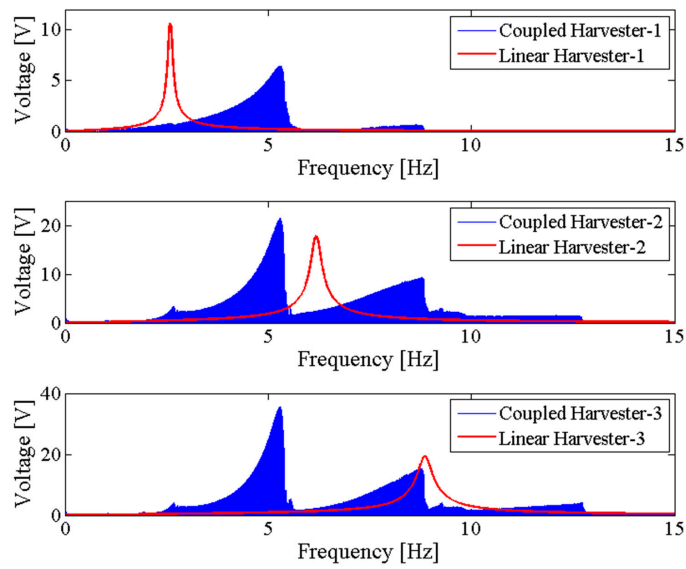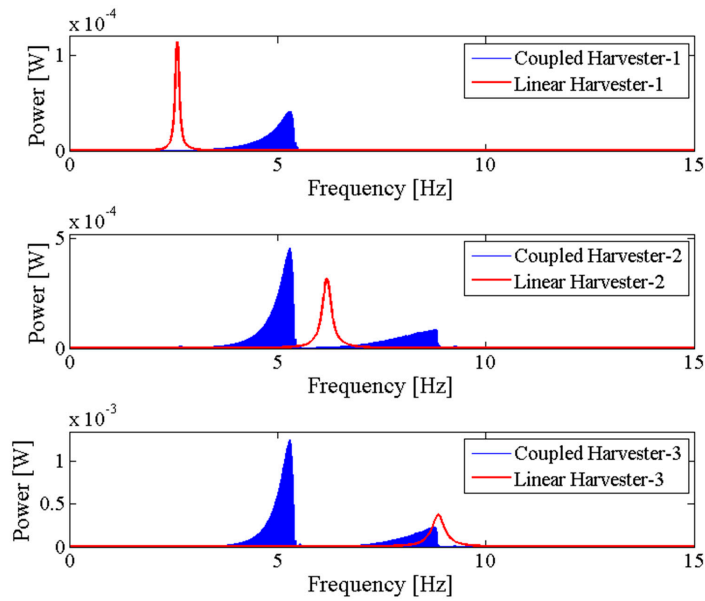
Figure 10. Output voltage of the NPEHS-2.

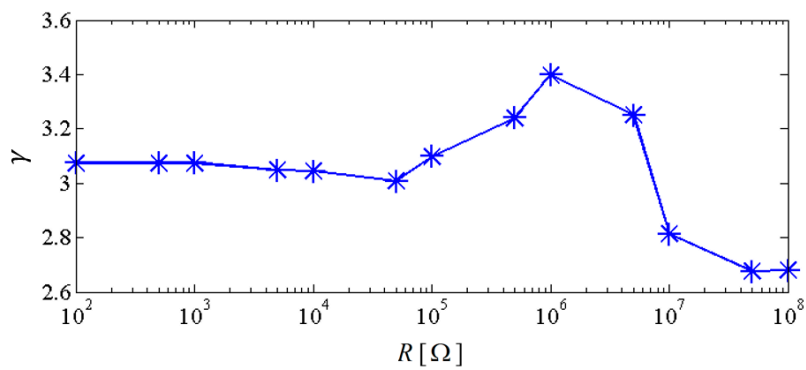**Figure 11.** Output power of the NPEHS-2.

Figure 12. Output power area ratio of the NPEHS-2 versus load resistance.

4. Nonlinear Dynamic Analysis

Above results verify the energy harvesting enhancement of the presented NPEHS with two or three energy harvesters. In order to reveal its dynamic mechanism, nonlinear dynamic analysis is provided below. Figure 13 shows the bifurcation diagram of response voltages of the NPEHS-1 under zero initial conditions versus the excitation level. The excitation level ranging from 0 to 1.8 g is the control parameter to numerically simulate the stable response voltage of the NPEHS-1 with the excitation frequency of 5 Hz. It is found from Figure 13 that the NPEHS-1 may undergo periodic and chaotic responses along with the increase of the excitation level, which demonstrates its strong nonlinearity [66,67,71–73]. In purpose of checking these nonlinear dynamic response characteristics, the phase plane portrait of the response displacement and the response velocity, and its Poincare map, the time-domain output voltage and its spectrogram via fast Fourier transformation (the excitation frequency is 5 Hz) are shown in Figures 14–21. In addition, the Poincare map is drawn by black dots.
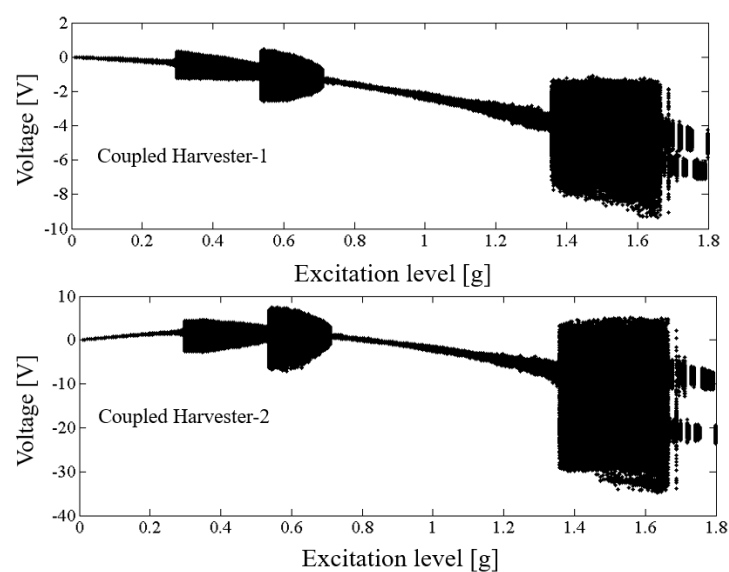

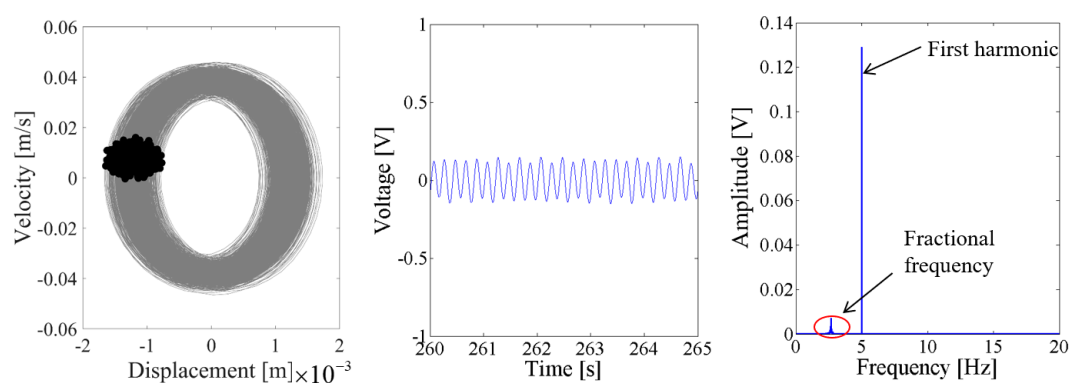**Figure 13.** Bifurcation diagram of response voltages versus excitation levels.

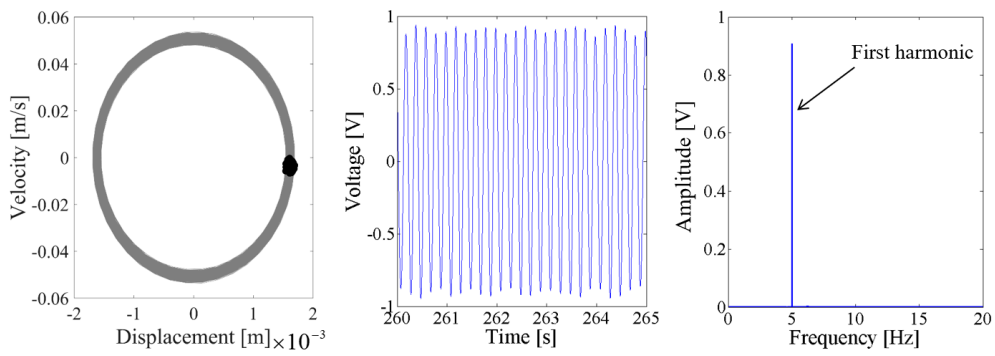**Figure 14.** Dynamic responses of the coupled harvester-1 for the excitation level of 0.1 g.

Figure 15. Dynamic responses of the coupled harvester-2 for the excitation level of 0.1 g.
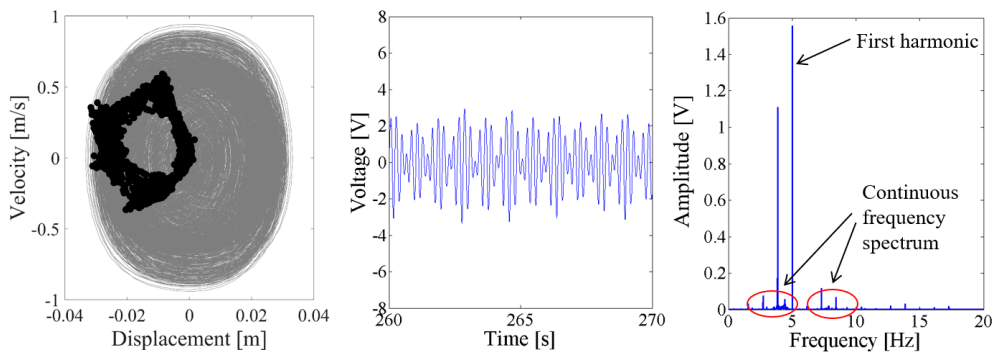

Figure 16. Dynamic responses of the coupled harvester-1 for the excitation level of 0.6 g.

Figure 17. Dynamic responses of the coupled harvester-2 for the excitation level of 0.6 g.

Figure 18. Dynamic responses of the coupled harvester-1 for the excitation level of 0.9 g.

Figure 19. Dynamic responses of the coupled harvester-2 for the excitation level of 0.9 g.

Figure 20. Dynamic responses of the coupled harvester-1 for the excitation level of 1.5 g.
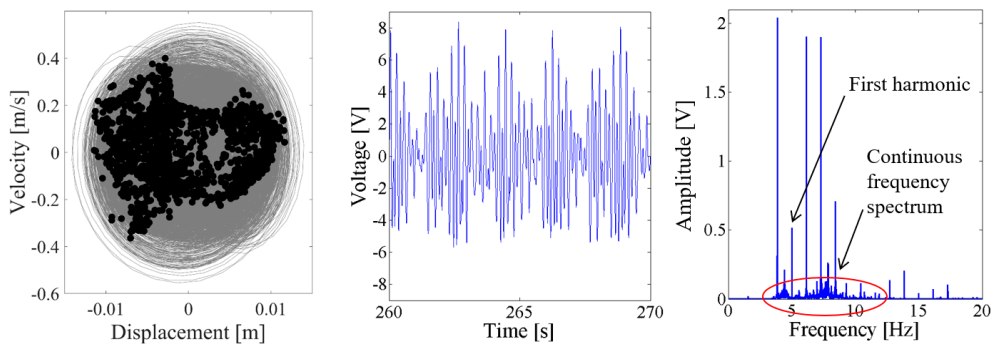

Figure 21. Dynamic responses of the coupled harvester-2 for the excitation level of 1.5 g.
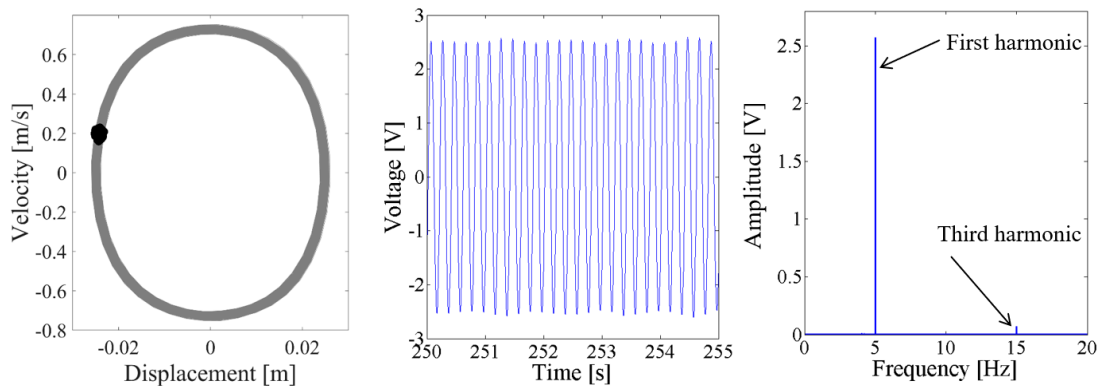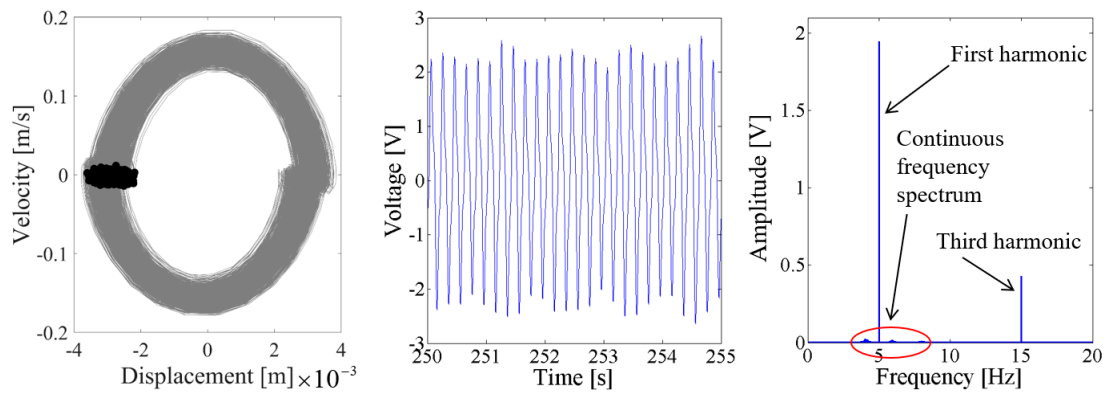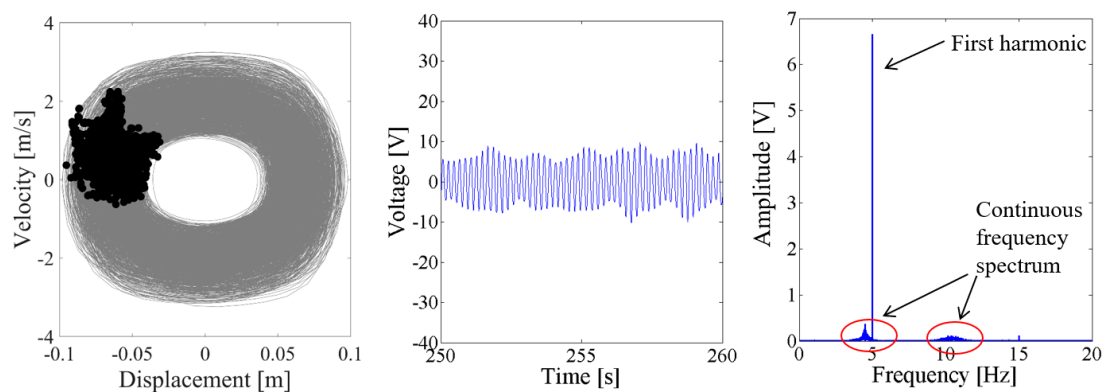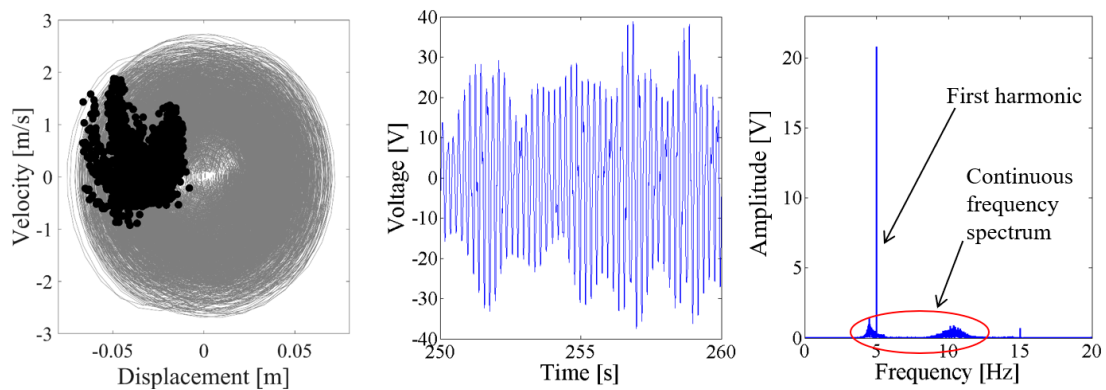
When the excitation level is 0.1 g, Figures 14 and 15 show that the output voltage of the coupled harvester-2 is larger than the coupled harvester-1, and the response voltage of the former is singly periodic. However, the Poincare map in the phase trajectory of the coupled harvester-1 consists of a series of discrete dots, as shown in the first plot of Figure 14. Its time-domain output voltage is the sine curve with fluctuating. The corresponding spectrum in Figure 14 shows that the fundamental harmonic is the uppermost component, while there is a non-ignorable 2.67 Hz fractional frequency component which modulates the fundamental harmonic.

As the excitation level increased to 0.6 g, the dynamic response of the NPEHS-1 is quite different with that when the excitation level is 0.1 g. In Figure 16, there are a lot of sub-harmonics and super-harmonics in the response voltage of the coupled harvester-1, as shown in the spectrum.

Meanwhile, there are more different discrete dots in the Poincare map of the phase trajectory for the coupled harvester-2, as shown in Figure 17. In this case, the response of the coupled harvester-2 can be considered as chaotic response, which is confirmed by its spectrum.

As the excitation level is further increased to 0.9 g, the spectrum in both Figures 18 and 19 show that there are the fundamental harmonic and the third harmonic in the response voltage of the two coupled energy harvesters. The Poincare map of the phase trajectory of the coupled harvester-1 looks like a fixed dot. This means that the response of the coupled harvester-1 is periodic, and there are no obvious sub-harmonics in the response voltage. However, there are continuous frequency components in the spectrum of the output voltage of the coupled harvester-2, and the fundamental harmonic is still the major component. The Poincare map of the phase trajectory of the coupled harvester-2 consists of a series of close dots, as the results shown in Figure 19.

When the excitation level is increased to 1.5 g, the response voltage is modulated by an infinite number of sub-harmonics and super-harmonics, because there are continuous frequency components in the spectrum of Figures 20 and 21. The corresponding Poincare map of phase trajectory consists of a lot of discrete dots. Therefore, the responses of the NPEHS-1 at 1.5 g excitation are chaotic.

Above analysis demonstrates that the nonlinear dynamic response characteristics of the NPEHS change along with the excitation conditions, and its response may be periodic or chaotic depending on the excitation conditions and initial conditions. Meanwhile, the fundamental harmonic is an important component in the response voltage and the response displacement, and there are sub-harmonics and super-harmonics under some excitation conditions. These features can be used to enhance energy harvesting and sensing in the further study.

5. Conclusions

As an alternative nonlinear energy harvesting technique, a novel nonlinear piezoelectric energy harvesting system without magnets is presented in the purpose of enhancing vibration energy harvesting performance. A theoretical model is derived based on Euler-Bernoulli beam theory, piezoelectric theory, Kirchhoff's law and the relevant geometrical relationship to predict the energy harvesting performance. Based on the appropriate design parameters, the output power area of the presented nonlinear system with two and three energy harvesters are 268.8% and 339.8% of their corresponding linear counterparts, respectively. This verifies that the presented nonlinear system can improve the energy harvesting efficiency under some specific conditions. In addition, nonlinear dynamic response characteristics are investigated by using the bifurcation diagram, the Poincare map of the phase trajectory, and the spectrum of the output voltage via fast Fourier transforms. The fundamental harmonic is found to be one main component of the response voltage, and sub-harmonics and super-harmonics are also found under some excitation conditions. This study focuses on the design, modeling and dynamic analysis of a novel nonlinear energy harvesting system for enhanced vibration energy harvesting. In the next step, further studies may focus on optimizing the number of energy harvesters, performing experiments and presenting the interface circuit for maximizing the energy harvesting performance.

Author Contributions: S.Z. presented the energy harvesting system, and derived the theoretical model, and wrote the paper. B.Y. and D.J.I. helped to check the theoretical model and simulations, and also helped to revise the paper.

Appendix A

Piezoelectric equations and boundary conditions:

The piezoelectric constitutive equations are used to describe the electromechanical behavior, defined as [3,74,75]:

$$T = c_{11}^E S - e_{31}E \tag{A1}$$

$$D = e_{31}S + \varepsilon_{33}^S E \tag{A2}$$

where T and S are the mechanical stress and the mechanical strain, respectively; E and D are the electric intensity and the electric displacement, respectively; e_{31} is the electromechanical coupling coefficient; c_{11}^E is the elasticity modulus measured in the zero electric field; c_{33}^S presents s the piezoelectric material permittivity constant at zero strain condition.

At the clamped end, the displacement and the angle of rotation should be zero, which results in the following two equations for the boundary conditions:

$$(\phi(0))_1 = 0 \tag{A3}$$

$$(\phi(0))'_1 = 0 \tag{A4}$$

Since the linear piezoelectric energy harvester is assumed to meet Euler-Bernoulli assumptions, the continuous condition of the displacement, the angle of rotation, the bending moment and the shear force are defined as:

$$(\phi(L_p))_1 = (\phi(L_p))_2 \tag{A5}$$

$$(\phi(L_p))'_1 = (\phi(L_p))'_2 \tag{A6}$$

$$EI_1(\phi(L_p))''_1 = EI_2(\phi(L_p))''_2 \tag{A7}$$

$$EI_1(\phi(L_p))'''_1 = EI_2(\phi(L_p))'''_2 \tag{A8}$$

At the free end, the tip mass block should be fully considered [35,66], and the boundary conditions are expressed as:

$$EI_2(\phi(L))''_2 - \omega^2 M_{tip}L_c(\phi(L))_2 - \omega^2(I_t + M_{tip}L_c^2)(\phi(L))'_2 = 0 \tag{A9}$$

$$EI_2(\phi(L))'''_2 + \omega^2 M_{tip}(\phi(L))_2 + \omega^2 M_{tip}L_c(\phi(L))'_2 = 0 \tag{A10}$$

where I_t is the rotary inertia of the tip mass block.

References

1. Roundy, S.; Wright, P.K. A piezoelectric vibration based generator for wireless electronics. *Smart Mater. Struct.* **2004**, *13*, 1131. [CrossRef]
2. Ho, S.C.M.; Li, W.; Wang, B.; Song, G. A load measuring anchor plate for rock bolt using fiber optic sensor. *Smart Mater. Struct.* **2017**, *26*, 057003. [CrossRef]
3. Erturk, A.; Inman, D.J. *Piezoelectric Energy Harvesting*; John Wiley & Sons: New York, NY, USA, 2011.
4. Luo, M.; Li, W.; Wang, B.; Fu, Q.; Song, G. Measurement of the Length of Installed Rock Bolt Based on Stress Wave Reflection by Using a Giant Magnetostrictive (GMS) Actuator and a PZT Sensor. *Sensors* **2017**, *17*, 444. [CrossRef] [PubMed]
5. Hou, Q.; Ren, L.; Jiao, W.; Zou, P.; Song, G. An improved negative pressure wave method for natural gas pipeline leak location using FBG based strain sensor and wavelet transform. *Math. Probl. Eng.* **2013**, *2013*. [CrossRef]
6. Fu, H.; Chen, G.; Bai, N. Electrode Coverage Optimization for Piezoelectric Energy Harvesting from Tip Excitation. *Sensors* **2018**, *18*, 804. [CrossRef] [PubMed]
7. Tao, K.; Tang, L.; Wu, J.; Lye, S.W.; Chang, H.; Miao, J. Investigation of multimodal electret-based MEMS energy harvester with impact-induced nonlinearity. *J. Microelectromech. Syst.* **2018**, *27*, 276–288. [CrossRef]

8. Erturk, A.; Inman, D.J. An experimentally validated bimorph cantilever model for piezoelectric energy harvesting from base excitations. *Smart Mater. Struct.* **2009**, *18*, 025009. [CrossRef]

9. Song, G.; Li, H.; Gajic, B.; Zhou, W.; Chen, P.; Gu, H. Wind turbine blade health monitoring with piezoceramic-based wireless sensor network. *Int. J. Smart Nano Mater.* **2013**, *4*, 150–166. [CrossRef]

10. Ho, S.C.M.; Ren, L.; Li, H.N.; Song, G. A fiber Bragg grating sensor for detection of liquid water in concrete structures. *Smart Mater. Struct.* **2013**, *22*, 055012. [CrossRef]

11. Liu, Y.; Yang, X.; Chen, W.; Xu, D. A bonded-type piezoelectric actuator using the first and second bending vibration modes. *IEEE. Trans. Ind. Electron.* **2016**, *63*, 1676–1683. [CrossRef]

12. Song, G.; Li, W.; Wang, B.; Ho, S.C.M. A review of rock bolt monitoring using smart sensors. *Sensors* **2017**, *17*, 776. [CrossRef] [PubMed]

13. Feng, Q.; Kong, Q.; Jiang, J.; Liang, Y.; Song, G. Detection of Interfacial Debonding in a Rubber-Steel-Layered Structure Using Active Sensing Enabled by Embedded Piezoceramic Transducers. *Sensors* **2017**, *17*, 2001. [CrossRef] [PubMed]

14. Kong, Q.; Fan, S.; Bai, X.; Mo, Y.L.; Song, G. A novel embeddable spherical smart aggregate for structural health monitoring: Part I. Fabrication and electrical characterization. *Smart Mater. Struct.* **2017**, *26*, 095050. [CrossRef]

15. Liu, Y.; Yan, J.; Xu, D.; Chen, W.; Yang, X.; Tian, X. An I-shape linear piezoelectric actuator using resonant type longitudinal vibration transducers. *Mechatronics* **2016**, *40*, 87–95. [CrossRef]

16. Lu, G.; Li, Y.; Wang, T.; Xiao, H.; Huo, L.; Song, G. A multi-delay-and-sum imaging algorithm for damage detection using piezoceramic transducers. *J. Intell. Mater. Syst. Struct.* **2017**, *28*, 1150–1159. [CrossRef]

17. Luo, M.; Li, W.; Wang, J.; Wang, N.; Chen, X.; Song, G. Development of a Novel Guided Wave Generation System Using a Giant Magnetostrictive Actuator for Nondestructive Evaluation. *Sensors* **2018**, *18*, 779. [CrossRef] [PubMed]

18. Li, W.; Ho, S.C.M.; Patil, D.; Song, G. Acoustic emission monitoring and finite element analysis of debonding in fiber-reinforced polymer rebar reinforced concrete. *Struct. Health Monit.* **2017**, *16*, 674–681. [CrossRef]

19. Cha, Y.; Hong, J.; Lee, J.; Park, J.M.; Kim, K. Flexible piezoelectric energy harvesting from mouse click motions. *Sensors* **2016**, *16*, 1045. [CrossRef] [PubMed]

20. Wickenheiser, A.M. Eigensolution of piezoelectric energy harvesters with geometric discontinuities: Analytical modeling and validation. *J. Intell. Mater. Syst. Struct.* **2013**, *24*, 729–744. [CrossRef]

21. Zhou, S.; Chen, W.; Malakooti, M.H.; Cao, J.; Inman, D.J. Design and modeling of a flexible longitudinal zigzag structure for enhanced vibration energy harvesting. *J. Intell. Mater. Syst. Struct.* **2017**, *28*, 367–380. [CrossRef]

22. Wang, X.; Shi, Z.; Wang, J.; Xiang, H. A stack-based flex-compressive piezoelectric energy harvesting cell for large quasi-static loads. *Smart Mater. Struct.* **2016**, *25*, 055005. [CrossRef]

23. Song, R.; Shan, X.; Lv, F.; Xie, T. A Novel Piezoelectric Energy Harvester Using the Macro Fiber Composite Cantilever with a Bicylinder in Water. *Appl. Sci.* **2015**, *5*, 1942–1954. [CrossRef]

24. Liang, J.; Liao, W.H. Improved design and analysis of self-powered synchronized switch interface circuit for piezoelectric energy harvesting systems. *IEEE. Trans. Ind. Electron.* **2012**, *59*, 1950–1960. [CrossRef]

25. Lan, C.; Tang, L.; Harne, R.L. Comparative methods to assess harmonic response of nonlinear piezoelectric energy harvesters interfaced with AC and DC circuits. *J. Sound Vib.* **2018**, *421*, 61–78. [CrossRef]

26. Zou, H.; Zhang, W.; Li, W.; Wei, K.; Hu, K.; Peng, Z.; Meng, G. A broadband compressive-mode vibration energy harvester enhanced by magnetic force intervention approach. *Appl. Phys. Lett.* **2017**, *110*, 502001. [CrossRef]

27. Xu, Z.; Shan, X.; Yang, H.; Wang, W.; Xie, T. Parametric Analysis and Experimental Verification of a Hybrid Vibration Energy Harvester Combining Piezoelectric and Electromagnetic Mechanisms. *Micromachines* **2017**, *8*, 189. [CrossRef]

28. Harne, R.L.; Thota, M.; Wang, K.W. Bistable energy harvesting enhancement with an auxiliary linear oscillator. *Smart Mater. Struct.* **2013**, *22*, 125028. [CrossRef]

29. Yan, Z.; Lei, H.; Tan, T.; Sun, W.; Huang, W. Nonlinear analysis for dual-frequency concurrent energy harvesting. *Mech. Syst. Signal Process.* **2018**, *104*, 514–535. [CrossRef]

30. Daqaq, M.F.; Masana, R.; Erturk, A.; Quinn, D.D. On the role of nonlinearities in vibratory energy harvesting: A critical review and discussion. *Appl. Mech. Rev.* **2014**, *66*, 040801. [CrossRef]

31. Wei, C.; Jing, X. A comprehensive review on vibration energy harvesting: Modelling and realization. *Renew. Sustain. Energy Rev.* **2017**, *74*, 1–18. [CrossRef]

32. Yang, Z.; Zhu, Y.; Zu, J. Theoretical and experimental investigation of a nonlinear compressive-mode energy harvester with high power output under weak excitations. *Smart Mater. Struct.* **2015**, *24*, 025028. [CrossRef]

33. Fang, Z.; Zhang, Y.; Li, X.; Ding, H.; Chen, L. Complexification-Averaging Analysis on a Giant Magnetostrictive Harvester Integrated With a Nonlinear Energy Sink. *J. Vib. Acoust.* **2018**, *140*, 021009. [CrossRef]

34. Fang, Z.; Zhang, Y.; Li, X.; Ding, H.; Chen, L. Integration of a nonlinear energy sink and a giant magnetostrictive energy harvester. *J. Sound Vib.* **2017**, *391*, 35–49. [CrossRef]

35. Abdelkefi, A.; Barsallo, N. Comparative modeling of low-frequency piezomagnetoelastic energy harvesters. *J. Intell. Mater. Syst. Struct.* **2014**, *25*, 1771–1785. [CrossRef]

36. Stanton, S.C.; McGehee, C.C.; Mann, B.P. Reversible hysteresis for broadband magnetopiezoelastic energy harvesting. *Appl. Phys. Lett.* **2009**, *95*, 174103. [CrossRef]

37. Zhou, S.; Cao, J.; Erturk, A.; Lin, J. Enhanced broadband piezoelectric energy harvesting using rotatable magnets. *Appl. Phys. Lett.* **2013**, *102*, 173901. [CrossRef]

38. Deng, W.; Wang, Y. Systematic parameter study of a nonlinear electromagnetic energy harvester with matched magnetic orientation: Numerical simulation and experimental investigation. *Mech. Syst. Signal Process.* **2017**, *85*, 591–600. [CrossRef]

39. Sebald, G.; Kuwano, H.; Guyomar, D.; Ducharne, B. Simulation of a Duffing oscillator for broadband piezoelectric energy harvesting. *Smart Mater. Struct.* **2011**, *20*, 075022. [CrossRef]

40. Cottone, F.; Vocca, H.; Gammaitoni, L. Nonlinear energy harvesting. *Phys. Rev. Lett.* **2009**, *102*, 080601. [CrossRef] [PubMed]

41. Cheng, C.; Chen, Z.; Xiong, Y.; Shi, H.; Yang, Y. A high-efficiency, self-powered nonlinear interface circuit for bi-stable rotating piezoelectric vibration energy harvesting with nonlinear magnetic force. *Int. J. Appl. Electromagn.* **2016**, *51*, 235–248. [CrossRef]

42. Borowiec, M.; Rysak, A.; Betts, D.N.; Bowen, C.R.; Kim, H.A.; Litak, G. Complex response of a bistable laminated plate: Multiscale entropy analysis. *Eur. Phys. J. Plus* **2014**, *129*, 1–7. [CrossRef]

43. Lan, C.; Qin, W. Enhancing ability of harvesting energy from random vibration by decreasing the potential barrier of bistable harvester. *Mech. Syst. Signal Process.* **2017**, *85*, 71–81. [CrossRef]

44. Zhou, S.; Cao, J.; Liu, S.; Wang, W.; Lin, J. Modeling and experimental verification of doubly nonlinear magnet-coupled piezoelectric energy harvesting from ambient vibration. *Smart Mater. Struct.* **2015**, *24*, 055008. [CrossRef]

45. Stanton, S.C.; McGehee, C.C.; Mann, B.P. Nonlinear dynamics for broadband energy harvesting: Investigation of a bistable piezoelectric inertial generator. *Physica D* **2010**, *239*, 640–653. [CrossRef]

46. Gao, Y.; Leng, Y.; Fan, S.; Lai, Z. Performance of bistable piezoelectric cantilever vibration energy harvesters with an elastic support external magnet. *Smart Mater. Struct.* **2014**, *23*, 095003. [CrossRef]

47. Zhou, S.; Cao, J.; Inman, D.J.; Lin, J.; Liu, S.; Wang, Z. Broadband tristable energy harvester: Modeling and experiment verification. *Appl. Energy* **2014**, *133*, 33–39. [CrossRef]

48. Li, H.; Qin, W.; Lan, C.; Deng, W.; Zhou, Z. Dynamics and coherence resonance of tri-stable energy harvesting system. *Smart Mater. Struct.* **2015**, *25*, 015001.

49. Kim, P.; Son, D.; Seok, J. Triple-well potential with a uniform depth: Advantageous aspects in designing a multi-stable energy harvester. *Appl. Phys. Lett.* **2016**, *108*, 243902. [CrossRef]

50. Panyam, M.; Daqaq, M.F. Characterizing the effective bandwidth of tri-stable energy harvesters. *J. Sound Vib.* **2017**, *386*, 336–358. [CrossRef]

51. Leng, Y.; Tan, D.; Liu, J.; Zhang, Y.; Fan, S. Magnetic force analysis and performance of a tri-stable piezoelectric energy harvester under random excitation. *J. Sound Vib.* **2017**, *406*, 146–160. [CrossRef]

52. Zhou, S.; Zuo, L. Nonlinear dynamic analysis of asymmetric tristable energy harvesters for enhanced energy harvesting. *Commun. Nonlinear. Sci. Numer. Simul.* **2018**, *61*, 271–284. [CrossRef]

53. Zhou, S.; Cao, J.; Litak, G.; Lin, J. Numerical analysis and experimental verification of broadband tristable energy harvesters. *TM Tech. Mess.* **2018**. [CrossRef]

54. Leland, E.S.; Wright, P.K. Resonance tuning of piezoelectric vibration energy scavenging generators using compressive axial preload. *Smart Mater. Struct.* **2006**, *15*, 1413–1420. [CrossRef]

55. Shahruz, S.M. Design of mechanical band-pass filters for energy scavenging: Multi-degree-of-freedom models. *J. Vib. Control* **2008**, *14*, 753–768. [CrossRef]

56. Kim, I.H.; Jung, H.J.; Lee, B.M.; Jang, S.J. Broadband energy-harvesting using a two degree-of-freedom vibrating body. *Appl. Phys. Lett.* **2011**, *98*, 214102. [CrossRef]

57. Wu, H.; Tang, L.; Yang, Y.; Soh, C.K. A novel two-degrees-of-freedom piezoelectric energy harvester. *J. Intell. Mater. Syst. Struct.* **2013**, *24*, 357–368. [CrossRef]

58. Kuch, B.; Karami, M.A. Powering Pacemakers with a Nonlinear Hybrid Rotary-Translational Energy Harvester. In Proceedings of the 2014 ASME on International Design Engineering Technical Conferences and Computers and Information in Engineering Conference, Buffalo, NY, USA, 17–20 August 2014.

59. Liu, W.; Bade, A.; Formosa, F.; Wu, Y.P.; Agbossou, A. Novel piezoelectric bistable oscillator architecture for wideband vibration energy harvesting. *Smart Mater. Struct.* **2013**, *22*, 035013. [CrossRef]

60. Chen, L.; Jiang, W. Internal resonance energy harvesting. *J. Appl. Mech.* **2015**, *82*, 031004. [CrossRef]

61. Chen, L.; Jiang, W.; Panyam, M.; Daqaq, M.F. A broadband internally resonant vibratory energy harvester. *J. Vib. Acoust.* **2016**, *138*, 061007. [CrossRef]

62. Xu, J.; Tang, J. Modeling and analysis of piezoelectric cantilever-pendulum system for multi-directional energy harvesting. *J. Intell. Mater. Syst. Struct.* **2016**, *28*, 323–338. [CrossRef]

63. Li, H.; Yang, Z.; Zu, J.; Qin, W. Distributed parameter model and experimental validation of a compressive-mode energy harvester under harmonic excitations. *AIP Adv.* **2016**, *6*, 085310. [CrossRef]

64. Wei, C.; Jing, X. Vibrational energy harvesting by exploring structural benefits and nonlinear characteristics. *Commun. Nonlinear Sci. Numer. Simul.* **2017**, *48*, 288–306. [CrossRef]

65. Thompson, J.M.T.; Stewart, H.B. *Nonlinear Dynamics and Chaos*; John Wiley & Sons: New York, NY, USA, 2002.

66. Nayfeh, A.H.; Mook, D.T. *Nonlinear Oscillations*; John Wiley & Sons: New York, NY, USA, 2008.

67. Kovacic, I.; Brennan, M.J. *The Duffing Equation: Nonlinear Oscillators and Their Behavior*; John Wiley & Sons: New York, NY, USA, 2011.

68. Liao, Y.; Sodano, H.A. Model of a single mode energy harvester and properties for optimal power generation. *Smart Mater. Struct.* **2008**, *17*, 065026. [CrossRef]

69. Malakooti, M.H.; Sodano, H.A. Piezoelectric energy harvesting through shear mode operation. *Smart Mater. Struct.* **2015**, *24*, 055005. [CrossRef]

70. Zhou, S.; Hobeck, J.D.; Cao, J.; Inman, D.J. Analytical and experimental investigation of flexible longitudinal zigzag structures for enhanced energy harvesting. *Smart Mater. Struct.* **2017**, *26*, 035008. [CrossRef]

71. Inman, D.J. *Engineering Vibration*, 4th ed.; Prentice Hall: Upper Saddle River, NJ, USA, 2013.

72. Masana, R.; Daqaq, M.F. Energy harvesting in the super-harmonic frequency region of a twin-well oscillator. *J. Appl. Phys.* **2012**, *111*, 044501. [CrossRef]

73. Cao, J.; Zhou, S.; Inman, D.J.; Chen, Y. Chaos in the fractionally damped broadband piezoelectric energy generator. *Nonlinear Dyn.* **2015**, *80*, 1705–1719. [CrossRef]

74. Yan, B.; Wang, K.; Hu, Z.; Wu, C.; Zhang, X. Shunt damping vibration control technology: A review. *Appl. Sci.* **2017**, *7*, 494. [CrossRef]

75. Yang, Z.; Zhou, S.; Zu, J.; Inman, D.J. High-Performance Piezoelectric Energy Harvesters and Their Applications. *Joule* **2018**, *2*, 642–697. [CrossRef]